INVESTIGATION OF SUBSYNCHRONOUS OSCILLATIONS IN GRID CONNECTED TYPE-2 WIND FARM AND ITS MITIGATION USING STATCOM

Boopathi V P **Kumudini Devi R P**
Department of EEE, Anna University, Chennai, India

Ramanujam R
Department of EEE, SRM University, Chennai, India

Bharathi Dasan S G
Department of EEE, Sri Venkateswara College Of Engineering, Chennai, India

Abstract: *This paper explores the possibility of occurrence of subsynchronous resonance (SSR) in a system comprising a conventional induction generator-based Type-2 wind farm connected to a series-compensated line. The induction generator is equipped with rotor resistance controller (RRC) which cuts in when wind velocity exceeds the rated. A comprehensive small-signal model of the system that includes the controller is developed and used for the analysis. The subsynchronous oscillations considered are due to self-excitation, torsional interaction and transient torque amplification. The test system considered is IEEE first benchmark model (FBM) for subsynchronous resonance with synchronous generator replaced by aggregated wind farm. Eigenvalue analysis is employed to evaluate system-wind farm interaction. The analysis includes the impact of series compensation level, wind velocity and wind farm size on SSR. Eigenvalue analysis is validated electromagnetic transient simulations and fast Fourier transform (FFT) analysis. The contributions of this paper are: Type-2 wind farms are more susceptible to self-excited oscillation at normal (practical) compensation levels, mitigation of these self-excited oscillations by the STATCOM controller that is employed at the point of common coupling for reactive power compensation, thereby avoiding the necessity of other controllers (FACTS).*

Key words: *- SSR, eigenvalues, induction generator effect, torsional interaction, rotor resistance controller, wind turbine generator, wind farm and STATCOM.*

1. Introduction

Subsynchronous resonance (SSR) phenomenon in steam turbine-generator connected to series-compensated transmission line has been exhaustively reported in literature [1]-[4]. In recent years, the investigation of SSR phenomenon in wind farms connected to series-compensated transmission line has become the focus of interest. The first ever incident of SSR in wind farms occurred in Type-3wind farm connected to 345 kV series-compensated transmission line at Zorillo Gulf wind farm in Texas [5]-[7].Type-3 wind generators are doubly-fed induction generators with back- to-back power electronic converters in the rotor circuit [8]. As with fossil-fired units, wind generators radially connected to series-compensated transmission line are more prone to SSR problems [9]. Fixed speed wind turbines are simple and robust. Unfortunately, we cannot extract the maximum power available from the wind using fixed speed turbines [10]. However, the maximum power can be extracted using variable speed wind turbines. From system operation point of view, it is highly desirable that the wind farm generates rated output power continuously even when wind speed varies. One method to obtain rated power output under varying wind speed conditions above the rated wind velocity is by the application of Type-2 wind turbine generators (WTG). Type-2 WTG use variable external rotor resistance in the rotor circuit of the wound-rotor induction generator (IG) to manipulate torque-speed characteristics and to control the output power [11]. Currently major vendors supply Type-3 andType-4 WTGs. Some vendors, Suzlon (S88) and Vestas(V47 and V80) supply Type-2 WTGs[12-14].The cumulative installed capacity of wind power under North American Electric Reliability Corporation (NERC), Alaska Systems Coordinating Council (ASCC) and Hawaii is 45 GW by the end of 2010. Out of 45 GW, the installed capacity of Type-2 wind farms is 11%[14].

In reference [15], steady-state SSR of self- excited double-cage induction generators(Type-1) connected to series-compensated transmission line are analyzed and mitigation of SSR using SVC and TCSC are reported. Reference[16] highlights the potential of steady-state and transient SSR in a self-excited single-cage induction generator connected to a series-compensated transmission line. In a recent paper [17], the potential for steady-state and transient SSR in double-cage induction generator connected to series-compensated transmission line is investigated. References [18]-[20] present modelling, modal analysis and mitigation of SSR in a Type-3 wind farm connected to a series-compensated transmission line. Grid side converter of Type-4 wind farm act as a STATCOM and mitigates SSR of thermal power plants as reported in [21]. An overview of SSR problems that could be encountered in wind farms and analysis methods, modelling, the

impact of control parameters and mitigation methods are presented in [22], but the authors have not discussed the occurrence of SSR in Type-2 wind farms. The authors in [23] have demonstrated that Type-2 wind turbines are capable of damping the SSR that occurs in synchronous generator connected to series-compensated line.

The capabilities of Static Var Compensator (SVC) and Static Synchronous Compensator (STATCOM) in mitigating SSR have been studied for type-1 WTG based wind farms [24-26]. A STATCOM based controller to mitigate the SSR in Type-1 wind farm is proposed in Reference[27] and a subsynchronous damping controller to mitigate the torsional interaction is proposed in [28].The TCSC with subsynchronous damping controller effectively improves the damping of torsional modes are presented in [29]. References [30, 31], demonstrated that SSSC is effective in damping the SSR oscillations. It detunes the network natural frequency and it improves damping of torsional modes.

This paper analyses the potential of SSR in Type-2 wind farm connected to series-compensated line. To the authors' knowledge, such an investigation has not been reported in the literature. A detailed mathematical model of complete system is first developed. Then, the eigenvalue analysis is resorted to for steady-state SSR assessment. The results are corroborated with time-domain simulations and fast Fourier Transform analysis using PSCAD/EMTDC and MATLAB respectively. Torque amplification is analyzed using PSCAD/EMTDC. Finally, mitigation of SSR using STATCOM controller is discussed by modelling STATCOM with 48-pulse voltage source converter.

The paper is structured as follows: Section 2 presents the study system and mathematical model of complete system that includes Type-2 wind generator rotor resistance controller. Section 3 deals with induction generation effect and effect of variation of wind velocity, series compensation level and wind farm size on induction generator effect. Section 4 presents the analysis of torsional interaction. Section 5 presents the torque amplification. Section 6 presents the mitigation of SSR using STATCOM and section 7 concludes the paper.

2. System modelling

The modified first benchmark (MFBM) model is considered for analysis. The synchronous generator in the first benchmark model [32] is replaced by a Type-2 wind farm as shown in Fig. 1a. The wind farm consists of identical WTGs and collective behavior of a group of WTGs and cables are represented by an equivalent WTG and cable [33], [34]. The degree of series compensation k, in percentage is expressed as $X_c/(X_{sys}+X_{l1}+X_{t1})*100$, where X_c series capacitor reactance, X_{sys} system reactance between the end of the transmission line and infinite bus, X_{l1} transmission line reactance and X_{t1}reactance of transformer.

A. Induction Generator

The voltage equations of a type-2 induction generator [16] in a synchronous d-q reference frame can be written as follows:

$$\frac{1}{\omega_b}\frac{d}{dt}\Psi_{sd} = -R_s i_{sd} + \omega_s \Psi_{sq} - v_{sd} \quad (1)$$

$$\frac{1}{\omega_b}\frac{d}{dt}\Psi_{sq} = -R_s i_{sq} - \omega_s \Psi_{sd} - v_{sq} \quad (2)$$

$$\frac{1}{\omega_b}\frac{d}{dt}\Psi_{rd} = -(R_r + R_{ext})i_{rd} + s\omega_s \Psi_{rq} \quad (3)$$

$$\frac{1}{\omega_b}\frac{d}{dt}\Psi_{rq} = -(R_r + R_{ext})i_{rq} - s\omega_s \Psi_{rd} \quad (4)$$

where v_{sd} and v_{sq} are d-q axis voltages at induction generator terminal, Ψ_{sd}, Ψ_{sq}, Ψ_{rd} and Ψ_{rq} are d-q axis stator and rotor flux linkages and i_{sd}, i_{sq}, i_{rd} and i_{rq} are d-q axis stator and rotor currents respectively. R_s and $L_{s\sigma}$ are stator resistance and leakage inductance respectively. R_r, R_{ext} and $L_{r\sigma}$ are rotor resistance, external resistance and leakage inductance respectively and L_m is unsaturated magnetizing inductance. ω_s and ω_b are the synchronous speed in per unit and base speed in rad/s respectively.

The flux linkages are given by Eq. (5):

$$\begin{bmatrix}\Psi_{sd}\\ \Psi_{sq}\\ \Psi_{rd}\\ \Psi_{rq}\end{bmatrix} = \begin{bmatrix}L_s & 0 & L_m & 0\\ 0 & L_s & 0 & L_m\\ L_m & 0 & L_r & 0\\ 0 & L_m & 0 & L_r\end{bmatrix}\begin{bmatrix}i_{sd}\\ i_{sq}\\ i_{rd}\\ i_{rq}\end{bmatrix} \quad (5)$$

where $L_s = L_{s\sigma} + L_m \qquad L_r = L_{r\sigma} + L_m$

The electromagnetic torque is expressed as

$$T_e = L_m(i_{sd}i_{rq} - i_{rd}i_{sq}) \quad (6)$$

Equation (5) is substituted into equations (1)-(4) and expressed in state space form as

$$\dot{\boldsymbol{X}}_{IG} = \boldsymbol{A}_{IG}\boldsymbol{X}_{IG} + \boldsymbol{B}_{IG}\boldsymbol{U}_{IG} \quad (7)$$

where $\boldsymbol{X}_{IG} = \left[i_{sd}i_{sq}i_{rd}i_{rq}\right]^t, \boldsymbol{U}_{IG} = \left[v_{sd}v_{sq}00\right]^t$

B. Rotor Resistance Controller

The block-diagram of the rotor resistance controller [10] is shown in Fig.1 (b). The rotor resistance controller consists of cascaded PI controllers. The outer loop regulates the active power (P_s) and inner loop regulates the rotor current (i_r). The controller is disabled and R_{ext} is set to zero when the wind velocity, u is below rated.

From Fig. 1(b), the equations describing RRC are:

$$\dot{X}_{R1} = K_{i1}\left(P_s^* - P_s\right) \quad (8)$$

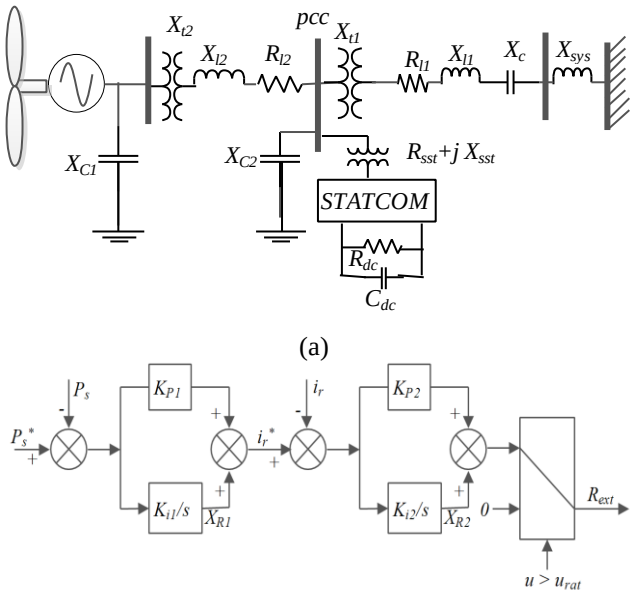

(a)

(b)

Fig. 1 (a) Modified First Benchmark Model System (b) RRC block-diagram

$$\dot{X}_{R2} = K_{i2}\left\{K_{p1}\left(P_s^* - P_s\right) + X_{R1}\right\} \tag{9}$$

$$R_{ext} = X_{R2} + K_{p2}\left\{X_{R1} + K_{p1}\left(P_s^* - P_s\right) - i_r\right\} \tag{10}$$

Here P_s^* is the rated stator power and P_s is the actual stator output power which is calculated as:

$$P_s = v_{sd} i_{sd} + v_{sq} i_{sq} \tag{11}$$

and i_r is calculated as:

$$i_r = \sqrt{{i_{rd}}^2 + {i_{rq}}^2} \tag{12}$$

Defining the state vector $\boldsymbol{X_{Rc}} = \begin{bmatrix} X_{R1} & X_{R2} \end{bmatrix}^t$

The entire power system is linearized around an operating point and cast in state space form in (13) and eigenvalues are computed and presented in Table 1.

$$\Delta \dot{\boldsymbol{X}} = \boldsymbol{A}\Delta\boldsymbol{X} + \boldsymbol{B}\Delta\boldsymbol{U} \tag{13}$$

3. Induction generator effect

The authors of this paper prefer the term self-excitation over induction generator effect (IGE) in the context of induction generators even though the latter seems to be more popular. The reason is that induction generator action (rotor driven ahead of stator rotating magnetic field) is present even during normal operation and is responsible for active power production. Therefore, the term IGE does not connote any abnormality in operation. On the other hand, the term self-excitation expresses unequivocally, an abnormal condition that occurs due to overall negative damping in the system consisting of the induction generator connected to the external network through an appropriate interface. The negative damping results when the magnitude of the equivalent resistance including the controlled external resistance exceeds the resistance of the stator circuit at one or more subsynchronous frequencies for which the slip is negative. This section presents the steady-state analysis of SSR to unearth self-excitation. The slip (s_1) at subsynchronous frequency is related to electric frequency of rotor speed (f_r) and the network natural frequency (f_n) through the following expression:

$$s_1 = \frac{f_n - f_r}{f_n} \tag{14}$$

Table 1: System eigenvalues

Modes	Eigenvalues	Frequency (Hz)
Network model	-6.65 ± 4448.64 i	708.02
	-6.69 ± 3694.65 i	588.02
	-15.42 ± 1935.08 i	308.00
	-22.24± 1180.91 i	187.95
Supersynchronous	-7.91 ± 453.26 i	72.14
Subsynchronous	-1.33 ± 299.93 i	47.73
Electromechanical	-26.23 ± 28.24 i	4.49
Torsional	-5.47 ± 4.68 i	0.74
System	-8.27	-
Control	-0.0005±0.003 i	0.0004

The slip s_1 is negative as f_r is greater than f_n. From the steady-state equivalent circuit of IG with RRC (shown in Fig. 2), the equivalent rotor resistance is negative ($(R_r+R_{ext})/s_1 < 0$). If the magnitude of this resistance exceeds the sum of IG stator resistance (R_s), wind farm power network (R_{l2}) and line resistance (R_{l1}), self-excitation results leading to sustained or growing oscillatory armature currents. This phenomenon is known as induction generator effect (IGE) [18]. As mentioned earlier, self-excitation will be a better terminology when induction generator is involved.

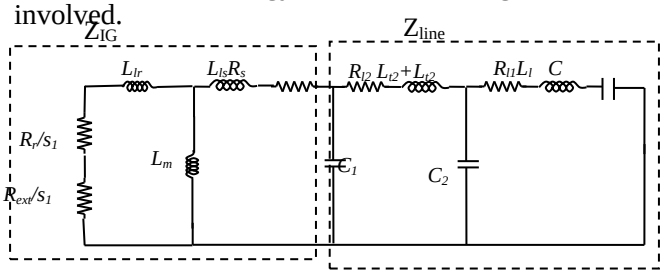

Fig. 2 Equivalent circuit of the system under subsynchronous frequency

A. Impact of wind velocity on subsynchronous mode

R_{ext} is zero from cut-in (6 m/s) to rated wind velocity (17 m/s). Table 1, summarizes slip, power output and R_{ext} for various wind velocities. This table reveals the effectiveness of RRC on output power regulation. As the wind velocity increases, R_{ext} and rotor speed have to increase to keep the power output at the rated value. In Table 2, s_1 is calculated from equation (14) for a compensation level of 20%. It is observed from Table 1 that an increase in wind velocity leads to an increase in the absolute value of R_{ext}/s_1 thereby $(R_r + R_{ext})/s_1$ will

increase negatively. Therefore, the net resistance of the system will decrease as the wind velocity increases. Hence, the damping of SSR mode will decrease as the wind velocity increases. Table 3 confirms this observation. It can be seen from this table that the damping of subsynchronous mode decreases with increase in wind velocity above the rated. The same observation holds good for Fig. 3(a) where movement of eigenvalues with respect to wind velocity for a compensation level of 20% is presented. The locus of subsynchronousmode enters negative damping region for a wind velocity of 24 m/s and instability due to self-excitation results. The damping of supersynchronous mode, electromechanical and torsional modes exhibit the opposite variation. The system is stable even at higher compensation levels for lower wind velocities as can be inferred from Table 4.

Table 2 Slip, Power Output, External Resistance and electric frequency of rotor speed of IG with RRC for different wind velocities for k= of 20%

u (m/s)	f_r(Hz)	$s_1=(f_n-f_r)/f_n$, f_n=12.26 Hz	Power Output (MW)	R_{ext}(pu)	R_{ext}/s_1
17	60.50	-3.9340	114.96	0.0000	0.0000
18	60.59	-3.9421	115.00	0.0015	-0.0004
19	60.94	-3.9703	115.00	0.0065	-0.0016
20	61.44	-4.0112	115.00	0.0139	-0.0035
21	62.03	-4.0598	115.00	0.0226	-0.0056
22	62.69	-4.1129	115.00	0.0322	-0.0078
23	63.37	-4.1685	115.00	0.0422	-0.0101
24	64.06	-4.2247	115.00	0.0523	-0.0124

B. Impact of compensation on subsynchronous mode

The network natural frequency, $f_n = f_o\sqrt{X_C/X_L}$ increases with increase in series compensation. The slip, s_1 decreases with increase in f_n from equation (14). The differential rate of increase of $(R_r+R_{ext})/s_1$ with increasing wind velocity forces a quicker march towards instability at lower compensation levels for wind velocities above rated. This is brought out clearly in Fig. 3 (b). From this figure, it can be observed that the movement of subsynchronous mode towards the right-half plane (RHP) is slow for the wind velocity of 16 m/s. Instability does not occur even for impractically high compensation levels (up to 90%). In contrast, for a wind velocity of 22 m/s and 30% compensation, the mode becomes marginally stable and instability results for 40% compensation. These are levels of compensation that are normally encountered in practice.

Table 4 Impact of SSR mode for compensation and lower wind velocities

k (%)	u = 8 m/s	u = 10m/s	u = 12 m/s
20	-4.55±300.00i	-4.55±300.00i	-4.55±300.00i
40	-4.11±268.12i	-4.11±268.22i	-4.10 ±268.24i
60	-3.69±243.95i	-3.69±243.97i	-3.69±244.00i
80	-3.27±223.62i	-3.27±223.64i	-3.27± 223.69i
90	-3.03±214.45i	-3.04±214.48i	-3.05 ±214.52i

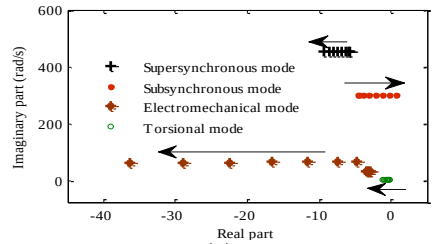

(a)

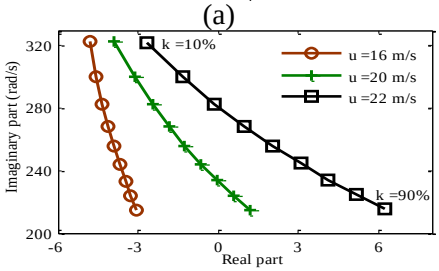

(b)

Fig.3 (a) Impact of wind velocity on different modes (b) Loci of subsynchronous mode for varying *k* and u

C. Impact of wind farm size on subsynchronous mode

As the wind farm size increases, IG equivalent stator resistance (R_s) and wind farm power network resistance decrease. Therefore, the net positive resistance (series-compensated line, wind farm power network, IG stator) of the system decreases with increasing wind farm size. It is observed from Table 5 that for a compensation level of 30% and wind velocity of 22 m/s, the SSR mode becomes unstable for a wind farm comprising100 units of WTG whereas it remains stable for a wind farm with 50 units of WTG. Therefore, wind farm size dictates the stability of SSR mode for a given compensation level and wind velocity.

Table 3 SSR mode of the system with RRC for above rated wind velocities

k (%)	u = 18 m/s	u = 19 m/s	u = 20 m/s	u = 21 m/s	u = 22 m/s	u = 23 m/s	u = 24 m/s
10	-4.71±322.62i	-4.37±322.56i	-3.88±322.50i	-3.31±322.45i	-2.67±322.45i	-2.06±322.41i	-1.45±322.43i
20	-4.40±300.03i	-3.87±299.97i	-3.13±299.93i	-2.26 ±299.91i	-1.33±299.93i	-0.39±300.00i	**0.53 ± 300.11i**
30	-4.13±282.76i	-3.44±282.71i	-2.47 ± 282.69i	-1.34 ± 282.71i	-0.15 ± 282.79i	**1.05 ± 282.93i**	**2.22 ± 283.13i**
40	-3.87±268.26i	-3.04±268.22i	-1.85 ± 268.22i	-0.48 ± 268.28i	**0.96±268.42i**	**2.40±268.64i**	**3.79 ± 268.94i**
60	-3.36±244.05i	-2.24±244.03i	-0.65 ± 244.08i	**1.17 ± 244.23i**	**3.08 ±244.52i**	**4.96 ±244.92i**	**6.76 ± 245.42i**
80	-2.85±223.75i	-1.44±223.75i	**0.56±223.87i**	**2.83±224.15i**	**5.18 ±224.62i**	**7.47 ±225.43i**	**9.62 ± 225.96i**
90	-2.59±214.59i	-1.03±214.61i	**1.18 ±214.78i**	**3.67 ±215.13i**	**6.24± 215.70i**	**8.72± 216.43i**	**11.04 ± 217.29i**

Table 5 SSR mode for different wind farm sizes with RRC at u=22 m/s

Wind farm size	30%	40%
50 units of WTG	-0.15 ±282.79i	**0.96±268.42i**
100 units of WTG	**0.80±256.01i**	**2.30±237.70i**
200 units of WTG	**2.22±228.24i**	**4.60±205.34i**

D. Electromagnetic transient simulation and FFT analysis

Electromagnetic transient simulation provides additional corroboration for eigenvalue analysis. It is carried out using PSCAD/EMTDC. The electromagnetic torque for progressive step changes in series compensation is shown in Fig. 4. The wind velocity chosen for the simulation is 22 m/s which is greater than the rated. From Fig. 4, it can be observed that the system is stable for jump up to 30% compensation and instability sets in for steps upwards of 40%. These observations are in agreement with the results obtained using eigenvalue analysis shown in Table 3. Fig. 5 captures the impact of wind velocity on the SSR mode for compensation level of 20%. It can be seen that as the wind velocity increases, there is a progressive deterioration in system damping and the system becomes unstable for the wind velocity of 24 m/s.

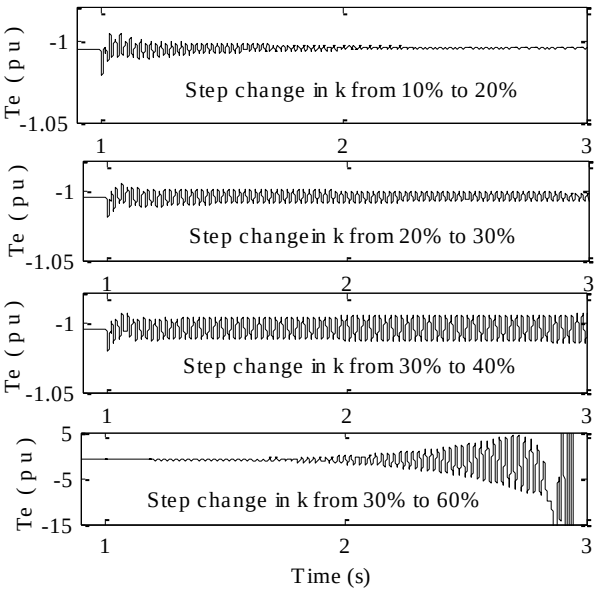

Fig. 4 Electromagnetic torques for different compensation levels and wind velocity of 22 m/s

FFT analysis is included here for quantitative corroboration of results from eigenvalue analysis. The candidate chosen for analysis is the electromagnetic torque shown in Fig. 6. FFT analysis conducted using the samples from 1 s to 1.5 s identifies the network modes as shown in Fig.6. The frequencies of supersynchronous, subsynchronous, electromechanical and torsional modes are identified using samples from a longer time span, since the time constants involved are larger due to mechanical system masses. Table 7 summarizes the frequencies obtained from eigenvalue and FFT analyses.

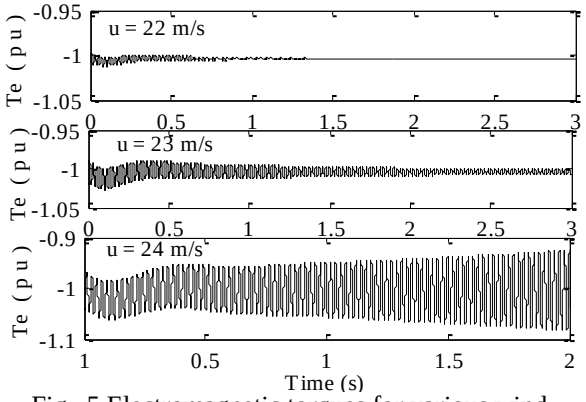

Fig. 5 Electromagnetic torques for various wind velocities and for compensation level of 20%

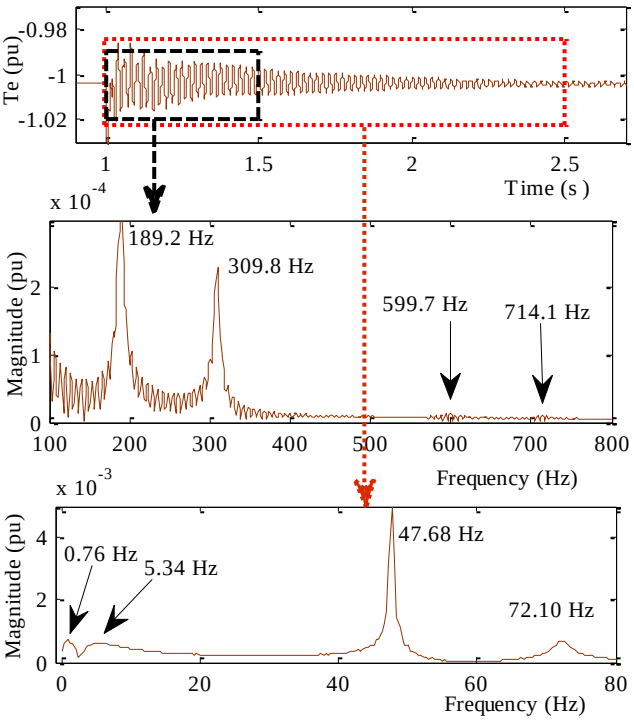

Fig. 6 FFT analysis of electromagnetic torque response at 20% compensation level and u= 22 m/s

Table 7 Frequencies of different modes from eigenvalue analysis and FFT analysis for k=20% and u= 22 m/s

Mode	FFT analysis	Eigenvalue analysis
Network mode-1	714.1 Hz	708.02 Hz
Network mode-2	599.7 Hz	588.02 Hz
Network mode-3	309.8 Hz	308.00 Hz
Network mode-4	189.2 Hz	187.95 Hz
Supersynchronous	72.10 Hz	72.14 Hz
Subsynchronous	47.68 Hz	47.78 Hz
Electromechanical	5.34 Hz	4.49 Hz
Torsional	0.76 Hz	0.74 Hz

4. Torsional interaction

Torsional interaction involves both the electrical and mechanical system dynamics. Generator rotor oscillations at a torsional mode frequency, f_m induce armature voltage components of subsynchronous frequency (f_o-f_m) and supersynchronous frequency (f_o+f_m). When the frequency of the subsynchronous component is close to electrical network natural frequency (f_n), the resultant subsynchronous current

will produce a rotor torque which is phased to sustain the rotor oscillations. If the component of subsynchronous torque in phase with rotor speed deviation equals or exceeds the inherent damping torque of the rotating system, the system will become self-excited. This interplay between the electrical and mechanical system is called torsional interaction [4].

Sensitivity of torsional mode for selected wind velocities was analysed. The analysis revealed that mode frequency is insensitive to compensation level for lower wind velocities. However, it exhibits a wide variation as the wind velocity is varied for a given compensation**.** For example, the frequency variation is 0.52 Hz to 1.65 Hz as the wind velocity changes from 10 m/s to 24 m/s for the compensation level of 20% is presented in Table 8. For the system considered variation of compensation from 10% to 90% causes variation in network natural frequency from 8 Hz to 26 Hz. The variation of torsional mode frequency is an order of lower magnitude and therefore, there is no risk of synchronous frequency complement of torsional mode frequency aligning with network natural frequency. Hence, self-excitation due to torsional interaction poses no problem. Even though the wind farm size is increased up to 150 units, torsional interaction is absent.

Table 8 Impact of wind velocity on Torsional mode

k(%)	u = 10 m/s	u = 16 m/s	u = 20 m/s	u = 22.5m/s	u = 24 m/s
20	-0.19±3.28i	-0.27±3.29i	-1.81±4.54i	-6.57±7.13i	-4.99±9.83i
40	-0.19±3.28i	-0.18±3.29i	-1.73 ±4.53i	-6.81±4.81i	-5.23±9.65i
60	-0.19±3.28i	-0.26±3.29i	-1.66±4.53i	-6.87±5.43i	-5.45±9.46i
80	-0.19±3.29i	-0.26±3.29i	-1.60± 4.53i	-6.31±4.34i	-5.66±9.24i
90	-0.19±3.29i	-0.25±3.29i	-1.58 ±4.53i	-5.79±4.10i	-5.76±9.13i

5. Torque Amplification (Transient SSR)

Transient SSR which occurs when there is a system disturbance in a series-compensated network can excite oscillatory torques of frequency f_0-f_n on the generator rotor. If this frequency is near f_m of any shaft section, the resulting shaft torques could be much larger than those produced by a three-phase fault in system without series capacitors. This is caused by the resonance between electrical and mechanical natural frequencies. These effects are referred as shaft torque amplification [3]. Time-domain digital simulation is the only approach to investigate transient torque phenomenon [39]. Fig. 7 shows the electromagnetic torque for two typical compensations when a three-cycle three-phase to ground (LLLG) fault is applied at the receiving end. The growing oscillations for a compensation of 40% indicate that there is a threshold compensation, before the onset of instability.

6 Mitigation of SSR

A 48-pulse VSC based STATCOM [27] is connected at pcc and its rating is selected so as to share a part of the reactive power requirement at pcc.

Fig. 8 shows the controller configuration [3] which consists of two PI controllers in series. The first PI controller is a voltage regulator, which generates the reactive reference current (i_R^*). It is then compared with the actual value of reactive component of the STATCOM current (i_R) to obtain the error which is then fed to the second PI controller to generate the required phase angle difference between STATCOM and pcc bus voltage (α). Two low pass filters are provided in the circuit to reduce the noise.

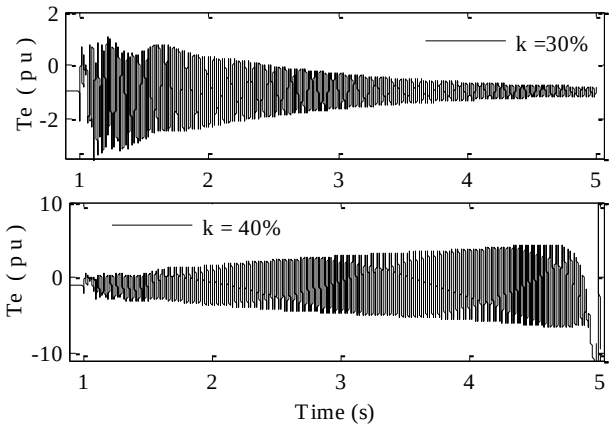

Fig. 7 Electromagnetic torque for LLLG fault at 1s for u=22m/s

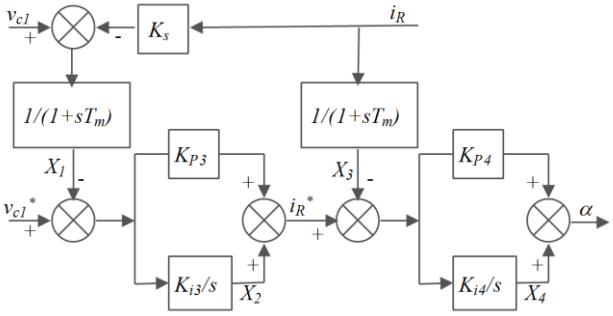

Fig. 8 STATCOM controller block diagram

The mathematical model of the STATCOM is developed considering the STATCOM currents (i_{std} and i_{stq}) and dc capacitor voltage (v_{dc}) as state variables on the STATCOM side. The equations are:

$$\dot{i}_{std} = \frac{-R_{sst}\,\omega_b}{X_{sst}} i_{std} + \omega_b i_{stq} + \frac{\omega_b}{X_{sst}}\left(e_{std} - v_{c1d}\right) \tag{14}$$

$$\dot{i}_{stq} = \frac{-R_{sst}\,\omega_b}{X_{sst}} i_{stq} - \omega_b i_{std} + \frac{\omega_b}{X_{sst}}\left(e_{stq} - v_{c1q}\right) \tag{15}$$

$$\dot{v}_{dc} = \frac{-\omega_b}{R_{dc}C_{dc}} v_{dc} - \frac{\omega_b}{C_{dc}} i_{dc} \tag{16}$$

where $i_{dc} = -\frac{3}{2}\left[m i_{std}\cos(\alpha+\theta) + m i_{stq}\sin(\alpha+\theta)\right]$

Here e_{std} and e_{stq} denote the STATCOM bus voltages in d-q reference frame. R_{sst} and X_{sst} represent the resistance and reactance of the interfacing transformer. i_{dc} denotes the current on the dc side of the

STATCOM, m represents the modulation index of the STATCOM converter and θ denoted PCC voltage angle.

Referring to Fig. 3, the equations for the STATCOM controller part can be written as:

$$\dot{X}_1 = \frac{1}{T_m}\left(-X_1 + v_{c1} - k_s i_R\right) \quad (17)$$

$$\dot{X}_2 = K_{i3}\left(v_{c1}^{*} - X_1\right) \quad (18)$$

$$\dot{X}_3 = \frac{1}{T_m}\left(-X_3 + i_R\right) \quad (19)$$

$$\dot{X}_4 = K_{i4}\left[K_{p3}\left(v_{c1}^{*} - X_1\right) + X_2 - X_3\right] \quad (20)$$

$$\alpha = X_4 + K_{p4}\left\{X_2 + K_{p3}\left(v_{c1}^{*} - X_1\right) - X_3\right\} \quad (21)$$

Here i_R and v_{c1} are calculated as:

$$i_R = \frac{-v_{c1d} i_{stq} + v_{c1q} i_{std}}{v_{c1}} \quad (22)$$

$$v_{c1} = \sqrt{{v_{c1d}}^2 + {v_{c1q}}^2} \quad (23)$$

Equations (17) – (20) can be linearized and represented in state space form.

A. Eigenvalue Analysis

This section initially presents the eigenvalue analysis carried out for the study system without STATCOM. The system is tested for wind velocities above u_{rat} (17 m/s) to incorporate RRC. Column I of Table 9 present the eigenvalues obtained for wind velocity (u) of 20 m/s and series compensation level (K) of 70%.

From Table 9, the subsynchronous mode is found to be stabilized by STACOM. Hence the study is further extended in analyzing the stability of the subsynchronous mode for variations in K and u. The results obtained are tabulated in Table 10.

From the columns corresponding to without STATCOM of Table 10, it can be noted that the destabilization of the subsynchronous mode occurs at low values of series compensation with increasing wind velocities indicating SSR potential in a type-2 WTG based wind farm. Thus, this paper explores the possibility of mitigating SSR in a type-2 WTG based wind farm by employing STATCOM.

Table 9, Eigenvalues for u = 20m/s and K = 70%

Modes	***u* = 20m/s, *K*=70%**	
	Without STATCOM	**STATCOM**
subsynchronous mode	**0.042 ± 234.6i**	-3.635 ± 237.072i
supersynchronous mode	-7.7 ± 518.6i	-8.501 ± 522.983i
other modes	-7.6 ± 3072.5i	-5.974 ± 17315.16i
	-7.9 ± 2318.5i	-10.638 ± 2468.064i
	-9.7 ± 1781.9i	-12.444 ± 1673.199i
	-13.1 ± 1028.0i	-5.416 ± 1467.428i
	-12.3 ± 32.8i	-12.481 ± 69.302i
	-1.6 ± 4.5i	-0.316 ± 5.258i
	-16.2	-16.861
	-0.06	-2.428
	-0.01	-0.0096 ± 0.015i
STATCOM controller modes		-4.135 ± 14.511i
		-479.272
		-500
		-6.03 ± 18158.494i

To affirm the capability of STATCOM controller in mitigating SSR, now the study system is analyzed with STATCOM by subjecting it to changes in series compensation levels and wind velocities above u_{rat}. The eigenvalues obtained for wind velocity of 20 m/s and series compensation level of 70% is shown in column II of Table 9 and the subsynchronous modes for various series compensation levels for $u > u_{rat}$ are presented in Table 10. From Table 9 and 10, we can observe that stabilization of subsynchronous mode is achieved with the addition of STATCOM. The locus of the damping ratio of the subsynchronous mode is traced to analyze the SSR mitigation by STATCOM over wide range of variations in series compensation level and wind velocity. The results obtained are shown in Fig. 9.

It is observed from Fig 9 that with increasing series compensation level, the damping ratio decreases and becomes negative without STATCOM. As the wind velocity increases the damping ratio becomes negative at lower values of series compensation in the absence of STATCOM. It can be seen that for the wind velocities of 22 m/s and 24 m/s the damping becomes negative at 30% and 20% series compensation levels respectively. But with the presence of STATCOM, the damping ratio increases with increasing compensation levels and decreases at extreme compensation levels but remains positive throughout the series compensation range considered. Therefore with STATCOM subsynchronous mode is stable for various

Table 10, Subsynchronus mode for variations in K and u

K (%)	u = 20m/s		u = 22m/s		u = 24m/s	
	Without STATCOM	STATCOM	Without STATCOM	STATCOM	Without STATCOM	STATCOM
10	-3.88±322.50i	-4.37 ± 323.06i	-2.67±322.45i	-3.72 ± 323.23i	-1.45±322.43i	-3.40 ± 323.57i
20	-3.13±299.93i	-4.13 ± 301.12i	-1.33 ± 300.26i	-3.44 ± 301.65i	**0.87 ± 300.48i**	-3.48 ± 302.47i
30	-2.47 ± 282.69i	-4.02 ± 284.59i	-0.15 ± 282.79i	-3.41 ± 285.48i	**2.22 ± 283.13i**	-3.97 ± 286.76i
40	-1.85 ± 268.22i	-3.97 ± 270.91i	**0.96±268.42i**	-3.50 ± 272.15i	**3.79 ± 268.94i**	-4.65 ± 273.89i
50	-1.12 ± 256.49i	-3.96 ± 259.07i	**2.24 ± 256.84i**	-3.65 ± 260.67i	**5.58 ± 257.58i**	-5.41 ± 262.86i
60	-0.65 ± 244.08i	-3.94 ± 248.61i	**3.08 ±244.52i**	-3.79 ± 250.54i	**6.76 ± 245.42i**	-6.12 ± 253.16i
70	**0.003 ± 235.15i**	-3.87 ± 239.24i	**4.19 ± 235.74i**	-3.81 ± 241.48i	**8.27 ± 236.87i**	-6.57 ± 244.48i
80	**0.56±223.87i**	-3.62 ± 230.89i	**5.18 ±224.62i**	-3.44 ± 233.33i	**9.62 ± 225.96i**	-6.24 ± 236.60i
90	**1.18 ±214.78i**	-2.59 ± 223.96i	**6.24± 215.70i**	-1.41 ± 226.18i	**11.04 ± 217.29i**	-2.71 ± 229.17i

compensation levels and wind velocities. Hence, STATCOM is effective in mitigating induction generator effect.

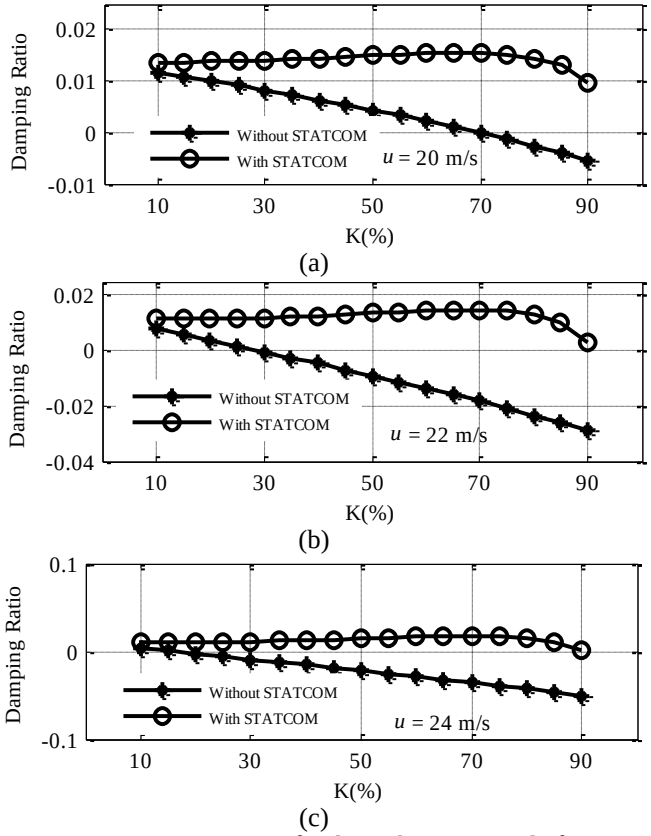

Fig. 9 Damping Ratio of Subsynchronous mode for various values of *K* for: (a) *u*=20m/s, (b) *u*=22m/s and (c) *u*=24m/s

B. Electromagnetic Transient Simulation

To validate the performance of the STATCOM controller in mitigating SSR with that of the eigenvalue analysis, the study system is examined for small signal SSR (step change in series compensation) through time-domain simulations using PSCAD/EMTDC. The study system is subjected to a step change in series compensation at a time instant of 1s for the following three cases to assess small signal SSR.

Case (i): u = 20 m/s, step change from 60% - 80%
Case (ii): u = 22 m/s, step change from 20% - 40%
Case (iii): u = 24 m/s, step change from 10% - 30%.

Responses of the electromagnetic torque of the study system with and without STATCOM are analyzed. The responses are shown in Fig. 10.

In Fig. 10, electromagnetic torque response of the system without STATCOM exhibit growing oscillations following a step change in compensation for case (i) whereas with STATCOM oscillations are damped out. This observation is in agreement with the results of eigenvalue analysis presented in Table 2 for wind velocity of 20 m/s and series compensation levels of 60% and 80%. Similar responses for cases (ii) and (iii) shown in Fig. 10. Thus, the performance of STATCOM in mitigating IGE for various operating conditions is validated.

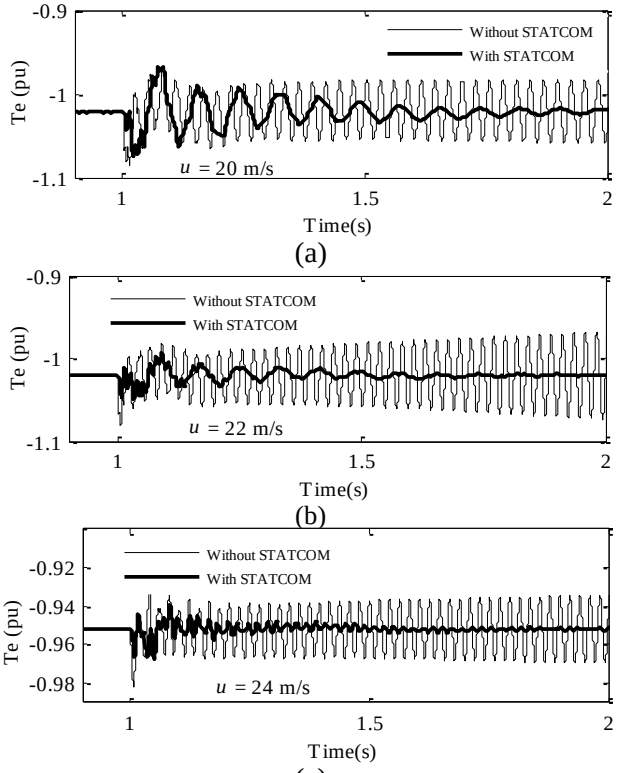

Fig. 10 Electromagnetic torque responses for: (a) case (i), (b) case (ii) and (c) case (iii)

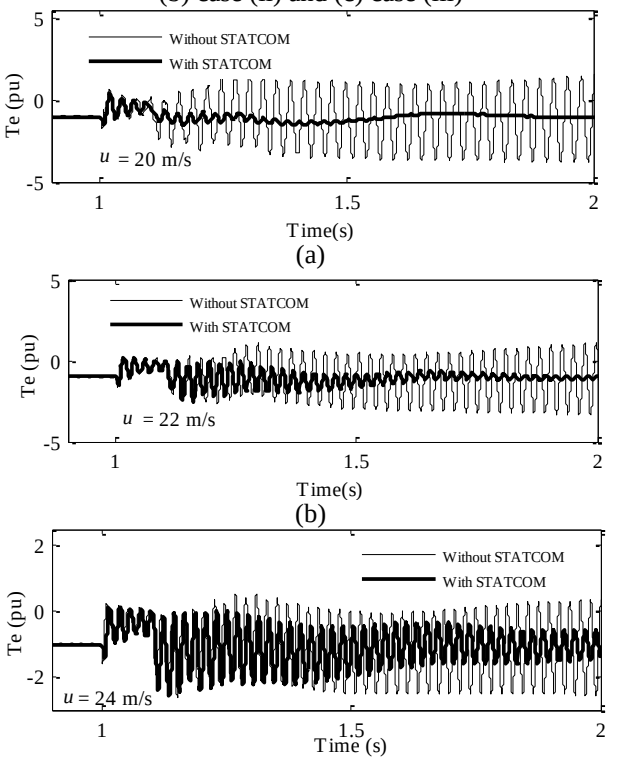

Fig. 11 Electromagnetic torque responses for a three phase fault for: (a) *u*=20 m/s, (b) *u*=22 m/s and (c) *u*=24m/s

C. Transient SSR

To analyze the system performance under transient condition, the study system is subjected to a three phase fault at the end of the line at a time instant of 1s for duration of 0.1s. The response of electromagnetic torque is illustrated in Fig.11. The series compensation levels are set at 60% for u = 20 m/s, 20% for u = 22 m/s and 10% for u = 24 m/s.

From Fig. 11 (a), it can be noted that with the inclusion of STATCOM the oscillations that occur following the application of fault are damped out gradually. Growing oscillations indicate the response in the absence of STATCOM. Figs. 11 (b) and (c), illustrate the responses obtained for u = 22 m/s and u = 24 m/s respectively on the application of fault.

Both eigenvalue analysis and electromagnetic transient simulation prove the effectiveness of STATCOM controller in mitigating SSR (both Small signal SSR and Transient SSR) over wide variation of series compensation levels as well as wind velocities when type-2 WTG based wind farm operate radially with a series-compensated transmission line.

7. Conclusions

This paper reports the investigation into the possibilities of occurrence of subsynchronous resonance in a Type-2 (with external rotor resistance control) wind farm. The wind farm is connected to the power system through a series-compensated line. The basic methodology is the eigenvalue analysis. The results from the eigenvalue analysis are validated by time-domain simulations using PSCAD/EMTDC, impedance model-based Nyquist criterion and FFT analysis. The sample system chosen for study is the first benchmark model for subsynchronous resonance with the 892.4 MVA machine replaced by a comparable size machine representing the windfarm. The major conclusions from the study are:

i. For the wind farm size considered, self-excitation is absent without rotor resistance control (type-1) for various combinations of wind velocities and compensation levels.
ii. With rotor resistance control (type-2) the stability of subsynchronous mode is dictated by series compensation level for given wind velocity. For practical values of compensation there is a threshold value for wind velocity above which the system is unstable.
iii. The frequency of the torsional mode is not in the proximity of the synchronous frequency complement of network natural frequency, thereby eliminating the possibility of torsional interaction.
iv. Compensation can influence the stability of transient SSR
v. STATCOM controller with simple voltage regulator is seen to effectively damp SSR oscillations, without the need for additional damping controllers, hence reducing cost and complexity. Inferences made from the results prove the performance of STATCOM in mitigating both small signal and transient SSR.

References

[1]Kundur, P.: 'Power system stability and control', (NewYork: McGraw-Hill, 1994).

[2] Padiyar, K. R.:'Analysis of subsynchronous resonance in power systems', (Boston: Kluwer Academic Publishers, 1999)

[3] IEEEsubsynchronous resonance working group of the system dynamic performance subcommittee:'Reader's guide to subsynchronous resonance', IEEE Trans. Power Syst., 1992,7(1), pp. 150 – 157

[4] IEEE Committee report:'Terms, definitions, and symbols for subsynchronous resonance oscillations' IEEE Trans. Power App. Syst., 1985,104, pp. 1326-1334

[5]North American Electric Reliability Corporation (NERC):'Subsynchronous interaction between series-compensated transmission lines and generation' Available online: www.nerc.com/pa/rrm/ea/Lessons%20Learned%20Document %20Library/ LL20110705 Sub-Synchronous Interaction.pdf, accessed 2013

[6]'ERCOT CREZ Project power conference, 2009' Available online: www.ercot.com/content/meetings/rpg-crez/ keydocs/2010/0126/ERCOT_CREZ_Project_Conference - Reed - 01-26-2010.pdf, accessed January 2017

[7] V-309, Elforsk rapport 11:29:'The impact of wind farms on subsynchronous resonance in power systems' Available online: http://www.elforsk.se/Programomraden/El--arme/Vindforsk/reports/reports_VFIII/reports_area_4/, accessed January 2017

[8] Farid, S. O., Unal, I., Rai, D., Mahseredjian, J.:'Utilizing DFIG -based wind farms for damping subsynchronous resonance in nearby turbine- generator', IEEE Trans.Power Syst., 2013, 28 (1), pp. 452-459

[9] Pourbeik, P., Koessler, R. J., Dickmander, D. L.,Wong, W.:'Integration of large wind farms in to utility grids (part2-performance issues)', Proc.IEEE Power Eng.Soc.GeneralMeeting Conf., 2003, pp.1520-1525

[10] Mohitsingh, Surya Santoso: 'Dynamic models for wind turbines and wind power plants', The University of Texas, subcontract report 2011.

[11] Burnham, D. J., Santoo, S., Muljadi, E.:'Variable rotor-resistance control of wind turbine generators', Proc.IEEE Power Eng.Soc.GeneralMeeting Conf., 2009, pp.1-6

[12] 'Wind Turbine Generator Model s88-2.1-MW', Available online: www.suzlon.com/pdf/product/Suzlon-S88-2.1MW-product-brochure.pdf, accessed January 2017.

[13] 'Wind Turbine Generator Model V47-660kW', Available online: www.creswindfarm.gr/site1 /Articles /V47_US.pdf, accessed January 2017.

[14] 'DOE ARRA project documentation, user support, and verification of wind turbine and plant models', Awarded To: EnerNex LLC, 2012, Available onlinehttp://www.osti.gov/scitech/biblio/1051403, accessed November 2013

[15] Varma, R. K.,Auddy, S., Semsedini, Y.:'Mitigation of subsynchronous resonance in a series-compensated wind farm using FACTS controllers',IEEE Trans. Power Del., July 2008, 23 (3), pp. 1645–1654
[16] Moharana, A., Varma, R. K.:'Sub synchronous resonance in single-cage self – excited – induction – generator – based wind farm connected to series – compensated lines: IET Gener. Transm.Distrib.,2011, 5 (12), pp. 1221 – 1232
[17] Moharana, A., Varma, R. K.:'SSR in Double-cage induction generator-based wind farm connected to series-compensated transmission line', IEEE Trans.Power Systems, 2013, 23 (8), pp. 2573-2583
[18]Lingling Fan, Rajesh Kavasseri, Chanxia Zhu and Zhixin Miao: 'Modeling of DFIG-based wind farms for SSR analysis', IEEE Trans.Power Del., October 2010, 25 (4), pp. 2073 – 2082
[19] Lingling Fan, Chanxia Zhu, Zhixin Miao, Minqiang Hu: 'Modal analysis of a DFIG-based wind farm interfaced with a series compensated network', IEEE Trans.Energy Convers., December 2011, 26 (4), pp. 1010 – 1020
[20] Lingling Fan, Zhixin Miao:'Mitigating SSR using DFIG-based wind generation',IEEE Trans. Sustain. Energy,July 2012,3 (3),pp.349-358
[21] Andres Enrique, Juan Manuel, Jorge Alberto: 'Subsynchronous resonance mitigation using variable – speed wind energy conversion systems', IET Gener. Transm. Distrib. 2013, 7(5), pp. 511-525.
[22] HoseinGhasemi, Gharehpetian, G. B., Seyed Ali Babavi, JamshidAghaei:,'Overview of subsynchronous resonance analysis and control in wind turbines', Renewable and sustainable energy reviews, 2013, Vol. 27, pp. 234-243
[23] Mikel De prada, Fernando Mancilla-David, Jose Luis Dominguez, et.al: 'Contribution of type-2 wind turbine to subsynchronous resonance damping', Electric power and energy systems, 2014, Vol. 55, pp. 714-722.
[24] Boopathi ,V .P., Kumudini Devi, R. P., Ramanujam, R.,and Muzamil Ahamed, R., "Analysis and mitigation of subsynchronous oscillations in a radially – connected wind farms", IEEE conference on Power and Energy Systems, March 2014.
[25] Akshaya Moharana, Rajiv. K.Varma and Ravi Seethapathy, "Subsynchronous Impact of Series Compensation on Induction Generator based Wind Farm", Electric Power components ans Systems, 4:11, pp.1041-1058: Taylor and Francis, 2013.
[26] Akshaya Kumar Moharana, "Subsynchronous resonance in wind farms", Ph.D dissertation, Univ.Western Ontario, Canada, 2012
[27] M. S. El-Moursi, B. Bak-Jensen, and M. H. Abdel-Rahman, 'Novel STATCOM controller for mitigating SSR and damping Power System Oscillations in a Series Compensated Wind Park', IEEE Transactions on Power Electronics, 2010, vol. 25, pp. 429-441
[28]Padiyar, K. R., NageshPrabu: 'Design and performance evaluation of subsynchronous damping controller with STATCOM', IEEE Trans. On power delivery,July 2006, Vol. 12 (3), pp. 1398-1396
[29] Joshi S. R., Kulkarni A. M., 'Analysis of SSR performance TCSC control schemes using a modular high bandwidth discrete-time dynamic control' IEEE Trans. On Power systems, May 2009, 24(2), pp. 840-848
[30] Farahani M., 'Damping of subsynchronous oscillations in power system using statis synchronous series compensator, 2012, 6(6), pp. 539-544
[31] Thirumalaivasan R., Janaki M., Nagesh Prabu, 'Damping of SSR using subsynchronous current suppressor with SSSC' IEEE Trans. On Power systems, Feb. 2013, 28(1), pp. 65-74
[32] IEEE Committee Report:'First benchmark model for computer simulation of subsynchronousresonance', IEEE Trans. Power App. Syst., June 1977, 95 (5), pp. 1565–1572
[33] Slootweg J. G.: 'Wind power modelling and impact on power system dynamics'. PhD thesis, Delft University of technology,2003. Available online
[34]Luis, M., Fernandez, José Ramon Saenz, Francisco Jurado:'Dynamic models of wind farms with fixed speed wind turbines', Renewable Energy, Elsevier, 2006, 31(8), pp. 1203–1230
[35]Lingling Fan, Zhixin Miao: 'Nyquist – stability – criterion – based SSR explanation for Type-3 wind generators', IEEE Trans. Energy Convers., 2012,27 (3), pp. 807-809
[36] Zhixin Miao: 'Impedance – model – based SSR analysis for Type 3 wind generator and series compensated network,' IEEE Trans. Energy Convers. 2012, 27 (4), pp. 984-991
[37]Pedra, J., Corcoles, F., Mojo, L.,Bogarra, S., Rolan, A.:'On fixed speed WT generator modelling for speed stability studies', IEEE Trans.Power Syst., 2012, 27 (1), pp. 397 – 406
[38] Luigi Dusonchet, Enrico Talaretti:'Effect of electrical and mechanical parameters on the transient voltage stability of a fixed speed wind turbine', Electric Power Systems Research, Elsevier, 2011,81(7), pp. 1308 – 1316
[39]Pillai, G. N., Arindam Ghosh, Joshi, A.:'Torsional oscillation studies in an SSSC compensated power system', Electric Power Systems Research, Elsevier, 2000, 55(1), pp. 57 – 65
[40] Narain, G., Hingorani, and LaszloGyugyi: 'Understanding FACTS: concepts and technology of flexible AC transmission systems', Wiley-IEEE Press, December 1999